Force Position Control for a Pneumatic Anthropomorphic Hand

Alexander Bierbaum, Julian Schill, Tamim Asfour and Rüdiger Dillmann
Institute for Anthropomatics
University of Karlsruhe (TH)
Karlsruhe, Germany
{bierbaum,schill,asfour,dillmann}@ira.uka.de

***Abstract*—Robot hands based on fluidic actuators are a promising technology for humanoid robots due to their compact size and excellent power-weight-ratio. Yet, such actuators are difficult to control due to the inherent nonlinearities of pneumatic systems. In this paper we present a control approach based on a simplified model of the fluidic actuator providing force and position control and further fingertip contact detection. We have implemented the method on the microcontroller of the human hand sized FRH-4 robot hand with 8 DoF and present results of several experiments, including system response and force controlled operation.**

I. Introduction

An important application for a humanoid robot is interaction with an environment designed for humans. Therefore, the robot should be able to manipulate and grasp objects. The desired manipulator system and especially the robot hand should provide sufficient power for grasping heavy objects, preciseness for dexterous manipulation and compliance for careful handling. For applications and experiments in humanoid robotics a lot of robot hands have been developed providing different characteristics in these categories. Among them are the four finger DLR-Hand II [1] which is driven by brushless DC motors situated in the hand, providing 3 DoFs per finger and position feedback. The NASA Robonaut hand [2] with 14 DoFs has been developed for space applications. Both hands are significantly larger in size than a human hand. For their advantageous power-weight-ratio the development of fluidic hands has been proposed. Famous representatives are the MIT-Utah hand [3] and later the Shadow hand using antagonistic air muscles as actuators [4]. Due to size and weight of the actuators these robot hands were not suitable for integration in a humanoid robot system. The pneumatic FRH-4 Hand which is also of the size of a human hand, has been developed at the Karlsruhe Research Center [5] as a prosthetic hand and development has been continued as a humanoid robot hand. The flexible fluidic actuators have been integrated directly to the finger joints and are operated using air as pneumatic medium. The actuators expand upon inflation causing a rotary motion of the joint. They may be operated pneumatically or with hydraulic media. With pneumatic operation closed circulation of the medium is not required, as the air may be released to the environment. Therefore pneumatic systems are easier to build. The air compressibility leads to a highly nonlinear control problem for position and force control, but provides the chance to design an inherently compliant system.

To control inflation and deflation of a pneumatic actuator electronically controllable valves are required which are divided into the categories of pressure regulators and switching valves. Pressure regulators allow precise pressure and flow control, as has been demonstrated e.g. in [6]. In [7] force and position control of a pneumatic robot arm has been reported which also uses pressure regulators. Unfortunately this valve type is currently too large to be integrated in a human sized hand. In [8] the position control system for a pneumatic robot arm using solenoid switching valves was presented. The authors used a PWM based valve control scheme [9]. A joint trajectory generator and pressure controller for a bipedal walking robot driven by artificial pneumatic muscles was presented in [10]. A bang-bang controller was used for controlling pressure and to actuate the switching valves.

A model-based torque and position control scheme for the flexible fluidic actuator type that is used in the FRH-4 hand has been presented in [11]. The method computes a target pressure as manipulated variable, the implementation of the underlying pressure control loop for switching valves has not been discussed. Results for integration of the controller with a single actuator were shown.

In this paper we present a force position control scheme for the pneumatic actuators of the FRH-4 robot hand. We introduce a simplified plant model based on the zero-load actuator characteristics to linearize major non-linearities of the system. Using this model we have developed a joint angle controller with torque limitation and a method for detecting fingertip contact from pressure and position sensor data. The algorithm has been implemented on a microcontroller system for controlling a robot hand with 8 DoFs in real-time. Results are given in terms of system responses from different experiments. An accompanying video shows demonstrations of the capabilities of the controlled hand.

This paper is organized as follows. In the next section the relevant details of the actuator and sensor system of the FRH-4 hand are given. In Sec. III we present the simplified plant model with control scheme and implementation. Further, we present experimental results in Sec. IV. Finally, we give a conclusion and an outlook on our future work in Sec. V.

II. Actuator and Sensor System

In this section we give a short description of the FRH-4 hand details and the sensor system we integrated for force position control.

A. Hand kinematics

The hand kinematics and standard system details have been reported in [5], therefore we will describe only details which have been altered for this work. The hand has eleven joints, two for each finger and one for the palm. The actuators of the ring and pinkie finger have been coupled, so that the hand has eight independent DoFs. The kinematic structure and the system architecture are shown in Fig. 1.

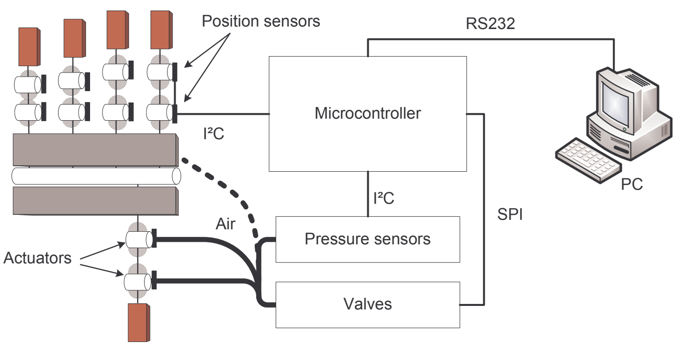

Fig. 1. Schematic system view and kinematics.

B. Actuators and valves

The hand is driven by flexible fluidic actuators. These are constructed from flexible bellows which expand when inflated and thus generate a torque around the joint. The actuators are inflated by compressed air at a maximum pressure of $4\,\mathrm{bar}$. Pneumatic operation has the advantage of providing compliance due to the air compressibility.

Two different types of actuators have been used. As smaller torques are needed in the distal joints, actuators with a diameter of $12\,\mathrm{mm}$ are used here, while larger actuators with $20\,\mathrm{mm}$ diameter have been attached to the proximal joints of the index and middle finger and to the joint in the palm. The different actuators exhibit different characteristics, which has to be considered in control design. The retraction force is generated by elastic rubber bands, which are attached to the bellows. Therefore active inflation of the bellow from a pressure reservoir produces different pressure vs. joint angle characteristics than during deflation, which is driven passively by the rubber band. To control the actuators we used 16 solenoid on/off valves. As this valve type is designed for switching operation the actuation variable is the switching time, i.e. the duration the valve is actuated. We found the minimal reproducable response time of these valves to be $3\,\mathrm{ms}$. If the valve is driven for a shorter time proper opening of the valve is not guaranteed.

Each actuator is connected to an inlet valve for inflation and an outlet valve for deflation, respectively. This configuration minimizes cross talk between the actuators in contrast to using a multiplex configuration with one valve for every actuator and a common valve pair for switching inlet and outlet.

The valves are controlled by the microcontroller via an integrated driver circuit connected to the SPI-bus.

C. Position sensors

To measure the actual joint angles we used magnetic rotary joint angle encoders of type AS5046 from *Austriamicrosystems*. These chips provide an absolute joint angle at a resolution of 12 bit over the range of $360°$. The measurement values are communicated via I^{2}C bus using the integrated interface of the chip and keeping the amount of wires and the size of the PCB small. Fig. 2(a) shows a mounted sensor on the hand. Every joint is equipped with a position sensor. Thus the configuration of the hand is fully observable although the hand is underactuated. As the sensors measure the orientation of a magnet in the joint, the zero point of the positions have to be set only once. Afterwards no initialization process is needed.

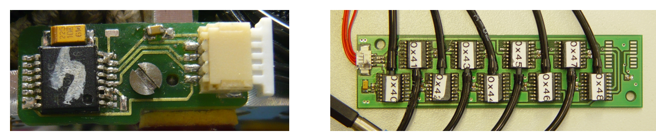

(a) Position sensor PCB (b) Pressure sensor PCB

Fig. 2. Sensor system of the robot hand.

D. Pressure sensors

Though position control can be achieved by only using joint angle encoders, the use of pressure sensors gives advantages. By interpreting the pressure values, conclusions to the actual torque in the joint can be drawn. Further it is possible to implement a cascaded control loop to enhance precision and stability of the control. The pressure sensors are mounted on a PCB measuring the actuator pressures as well as the pressure of the supply. The chip SM5822 from *Silicon Microstructures Inc.* has been used, which features an I^{2}C interface and provides temperature compensated and linearized values with a resolution of $3\,\mathrm{mbar}$. The sensors are available with calibration from the manufacturer. The PCB with the mounted sensors is shown in Fig. 2(b).

III. Force and Position Control

The actuator model is complex due to several nonlinear effects in the pneumatic system. First, the medium itself is compressible, therefore the joint angle and stiffness is not only affected by the internal pressure but also by external forces. Further, the actuator material and the retraction spring have viscoelastic force characteristics which have the effect of a hysteresis on the joint angle.

A. Theoretical model

A theoretical model for the actuator system has been discussed in [11]. This model approximates the characteristics of the actuator by the multilinear equation

$$M_A(\varphi, p) = a_0 + a_1 \cdot \varphi + a_2 \cdot p + a_3 \cdot \varphi \cdot p, \tag{1}$$

where p is the pressure in the actuator and φ is the actual joint angle. To obtain the torque acting upon the joint the disturbance torque M_{dist} has to be taken into account. Additionally torque components induced by friction and inertia act in the opposite direction resulting in the differential equation

$$J\ddot{\varphi} + D\dot{\varphi} = M_A(\varphi, p) + M_{\text{dist}} \tag{2}$$

The flexible actuator material exhibits a hysteresis and a drift due to viscoelastic behavior. This can be modeled via spring-damper elements which extend the first order component of Eq.1. The viscoelastic state A of a material is defined using coefficients K_E and K_R, time constants T_E and T_R for expansion E and relaxation R

$$\begin{cases} T_E\dot{A} = K_E \cdot (p - p_{\text{min}}) & : A < A_{\text{min}} \\ \dot{A} = 0 & : A_{\text{min}} \leq A \leq A_{\text{max}} \\ T_R\dot{A} + A = K_R \cdot p & : A > A_{\text{max}} \end{cases}$$

where

$$A_{\text{min}} = K_E \cdot (p - p_{\text{min}})$$
$$A_{\text{max}} = K_R \cdot p$$

The value A $[0 \ldots 1]$ is a creeping ratio, which influences the reset torque. With increasing A the reset torque is decreasing. In a similar way also the rubber band, which is attached to the actuator and is used as reset spring shows hysteresis and drift depending on its elongation. With the viscoelastic states of the actuator A_{Act} and the rubber band A_{Rbb} Eq. 1 becomes

$$\begin{aligned} M_A(\varphi, p) = & a_0 + a_1 \cdot (\varphi - A_{\text{act}} \cdot \Delta\varphi_{\text{Amax}} - A_{\text{Rbb}} \cdot \Delta\varphi_{\text{rMax}}) \\ & + a_2 \cdot p + a_3 \cdot \varphi \cdot p \end{aligned} \tag{3}$$

B. Model approximation

Since this model is complex and many parameters are uncertain and difficult to estimate individually for every actuator, we chose to consider the system in a lumped model. In such a model the main nonlinearities may be approximated using suitable functions.

From Eq. 1 follows that control of the actuator torque is achieved by controlling the pressure. We therefore characterized the actuator function between pressure and joint angle when no load is applied, see Fig. 3. Although this function is afflicted with hysteresis, we chose to not consider this component. Any control error resulting from this simplification should be compensated by closed loop control.

Thus we were looking for a function, which approximates the measurement data of the actuator. For the small actuators in the distal joints we found a usable fit $p(\varphi)_{dist}$ by applying a 4th order polynomial, while for the larger actuator in the proximal joints and in the palm a sum of two exponential functions gives a better approximation. The parameters for the function were estimated using the least-square method. Figures Fig.3(a) and Fig.3(b) show typical measurement plots and corresponding fit functions for the two actuator types. The transfer function must be fitted for every actuator individually which mainly arises from individual characteristics of the elastic rubber band.

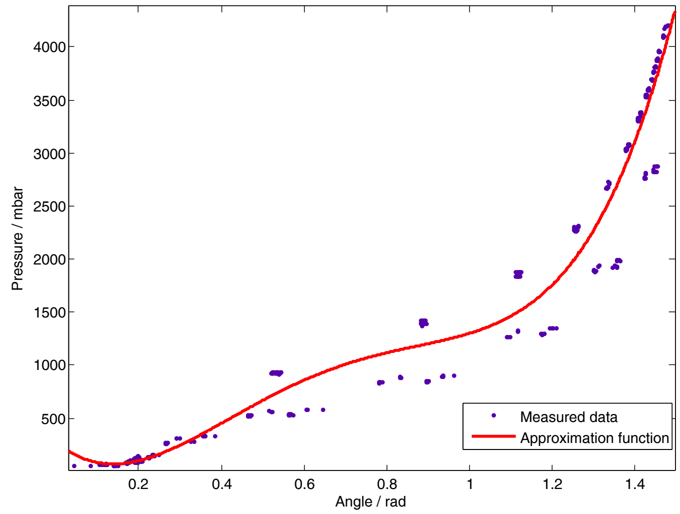

(a) Polynomial approximation for distal actuator.

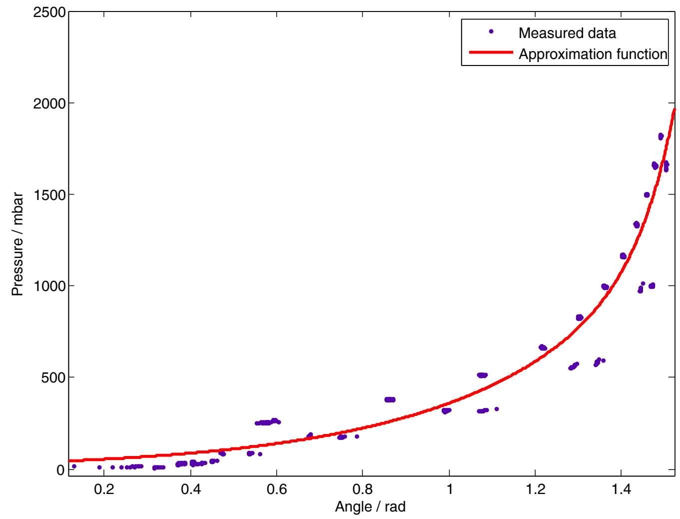

(b) Exponential approximation for proximal actuator.

Fig. 3. Actuator characteristic functions.

C. Control Algorithm

For joint angle control a cascaded controller with a pressure controller as inner loop is used. The pressure control directly affects joint torque.

We assume that the disturbance torque acting on the actuator is stationary during one control cycle. The joint angle controller uses the approximated function $p(\varphi)$ to compute a target pressure as output variable which is passed to the pressure controller. We compute a target pressure p_c from the target angle φ_c by extrapolating linearly $p(\varphi_c)$ from the zero-load case which gives

$$p_{\text{c}} = p_{\text{act}} + K_{\text{p}} \cdot \frac{dp(\varphi_{\text{c}})}{d\varphi} \cdot (\varphi_{\text{c}} - \varphi_{\text{act}})$$

where p_{act} and φ_{act} are the current pressure and joint measurement values. and K_{p} is the controller gain.

The target pressure p_{c} is input to the pressure controller which is designed as a proportional controller for a control difference $|\Delta p| > 100\text{mbar}$. For lesser control differences the switching time is fixed to the minimum value. The output variable of the pressure controller is the switching time of the valves. The sign of the output variable determines which valve of the actuator is operated, a positive value indicates operation of the inlet valve while a negative value indicates operation of the outlet valve. The valves have a minimum switching time of $3\,\text{ms}$. This minimum valve activation results in a maximum pressure difference of $50\,\text{mbar}$ for the distal actuator type and up to $20\,\text{mbar}$ for the proximal actuator which limits the achievable resolution of the control to these pressure differences. To decrease the effects of both actuator non-linearities, the minimum switching time and the unsymmetric transfer characteristics during inflation and deflation, we have decided to add a dead band limiter element which prevents oscillation around the target position.

Force control is achieved by limiting the maximum applied torque for each joint. This way stiffness of the joint may be adjusted and the force acting on a grasped object is restricted which is important for grasping of fragile objects. From Eq.3 follows

$$\frac{dM}{dp} = \text{const}, \tag{4}$$

and so limiting the actuator pressure linearily limits joint torque. Therefore, the output pressure command of the position controller is delimited to a maximum value

$$p_{\text{c,max}} = p(\varphi_{\text{act}}) + p_{\text{max}}, \tag{5}$$

where p_{max} is the maximum pressure the actuator should produce additional to the estimated zero-load pressure $p(\varphi_{\text{act}})$ at the actual joint position.

The structure of the position controller with force limiting is shown in Fig. 4. Limiting of force in the joint opening direction is not considered, as this force direction is only passively controlled by the elastic rubber bands.

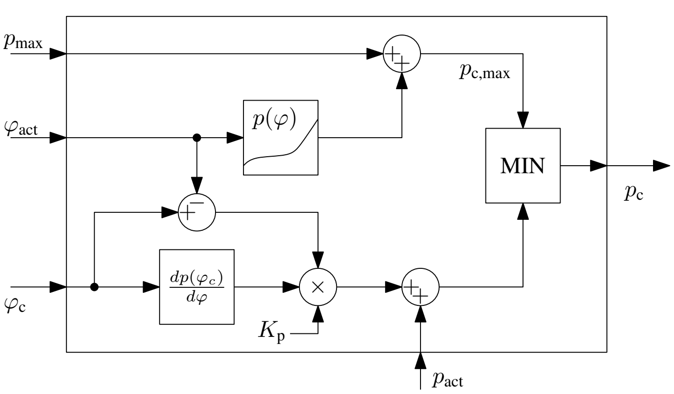

Fig. 4. Scheme of the force position controller.

D. Fingertip contact detection

By observing the actual pressure and the expected zero-load pressure $p(\varphi)$ at the current joint angle it is possible to detect contact between a finger and an obstacle or object. First the load pressure value is computed as

$$p_{\text{l}} = p_{\text{act}} - p(\varphi) \quad .$$

For a single-contact situation, considering only the contact at the fingertip we calculate a contact force value F_l proportional to the force F_M acting at the fingertips, Fig. 5(b). A computationally effective method for approximation of

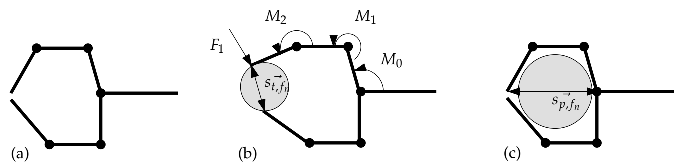

Fig. 5. Examples for a failed grasp, a successful precision grasp and a successful power grasp.

F_l is to calculate a weighted sum over the load pressure values and filter the result. Thus we obtain the contact force approximation F_l at a finger tip

$$F_l = \sum_{\text{n}=0}^{\text{n}} g_{\text{k}} p_{\text{l,k}} \quad , \tag{6}$$

with g_{k} being the weights for the joint torque contribution of $p_{\text{l,k}}$. The weights of joints close to the fingertip are set to a lesser value than the weights for more distant joints as the effective leverage at distant joints is greater. Because the load pressure of the palm joint actuator contributes to all fingers, the weight for this joint is chosen comparatively small to prevent crosstalk of contact force readings between fingers in contact and fingers not in contact.

A contact situation is detected by comparing F_l of a particular finger with a threshold value. Further, the forward kinematic model of the hand is deployed to distinguish contact between fingers, i.e. self-collision of the fingers, from contact between fingers and an external object.

The contact force approximation F_l may be also used to determine if a grasp was successful. For this application we use the forward kinematics of the hand to determine a distance vector $\vec{s_{\text{t,fn}}}$ between thumb and finger tips in case of precision grasp, or a distance vector $\vec{s_{\text{p,fn}}}$ between finger tips and palm in case of a power grasp. A grasp is determined successfull if a contact is detected at corresponding opposing fingers at a certain distance, see Fig. 5.

E. Implementation

The control algorithm was implemented on a PIC24H microcontroller from *Microchip Technology Inc.*. The software structure can be seen in Fig. 6. Using a time-based scheduling scheme, three threads are run in parallel. A measurement thread triggers data readback from the I^2C-Sensor every $15\,\text{ms}$. The control thread is also run at a $15\,\text{ms}$ time base and computes the controller output, i.e. the activation period of each valve of every actuator. It starts actuation of the respective valves if indicated by the result of the control algorithm. A third auxiliary thread checks timeouts for current actuated valves every 1 ms and deactivates them accordingly. On a lower execution level communication to a host PC via

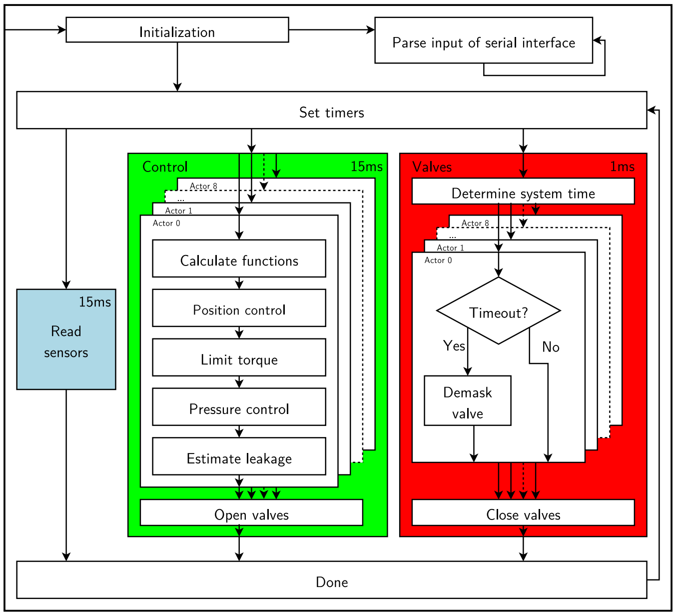

Fig. 6. Structure of microcontroller software implementation.

serial interface is realized. The communication interface allows controller configuration and monitoring of internal variables and sensor data.

IV. Experiments and Results

We present different experiments for demonstrating the performance of the tuned controller. We found a value of $K_p = 1.0$ applicable for all actuators. The approximated actuator characteristics $p(\varphi)$) have been acquired individually. During the experiments command values for angle position and moment and actual measurement values for angle position, pressure and moment were recorded synchronously.

A. Joint angle control

Different response plots of the proximal index acuator with no load applied are shown in Fig. 7. The step response in Fig. 7a shows that the target angle is reached in 0.5 s when closing the joint. Due to the lower reset force caused by the rubber band the joint opening process is slower and may take about 1.5 s for large angle differences. The bottom plot shows actuator moment and pressure. The peak observed in moment upon a step command is related to the delayed expansion of the actuator. The estimated moment value during steady-state is non-zero which is a consequence of the simplified model where hysteresis is neglected. Still, the cascaded controller reaches the setpoints with a mean error of 0.026 rad which is approximately 1.5 deg.

Fig. 7b shows the results for tracking a linear ramp function of the joint angle command. Here, the mean error has a value of 0.072 rad (approx.4.1 deg). It is also visible that the joint angle is limited to a minimum value. This is due to the active range of the rubber band which determines the reset force. The negative moment estimate during ramp descent is also a consequence of non-modeled hysteresis.
Fig. 7c shows the results for tracking a sine ramp function with a mean error of 0.023 rad (approx.1.3 deg).

B. Compliance by joint force limitation

In a different experiment we demonstrate the force control performance of the developed method. Therefore, the target position of an actuator was fixed to 0.7 rad while permitting a maximal load pressure of $p_{c,max}$ 2000 mbar. After the target position was reached, the external load pressure was manually increased by pressing against the joint until the end position was reached and releasing the external pressure again. The result plot in Fig. 8 clearly shows that the controller permanently increases the actuator pressure until $p_{c,max}$ is reached to keep the joint angle position during the interval $(7s < t < 10s)$. From $(10s < t < 30s)$ the applied external

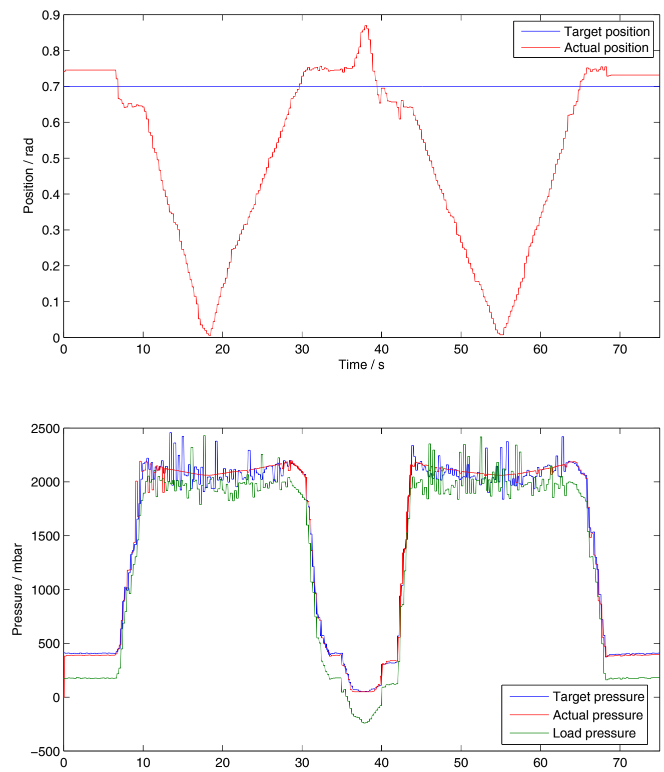

Fig. 8. Typical disturbance behavior of force position control.

load pressure and the internal air pressure outrange $p_{c,max}$ and the controller adapts in a compliant manner by releasing air and therefore deriving from the target joint angle. As soon as the external load decreases from $(18s < t < 30s)$, air is

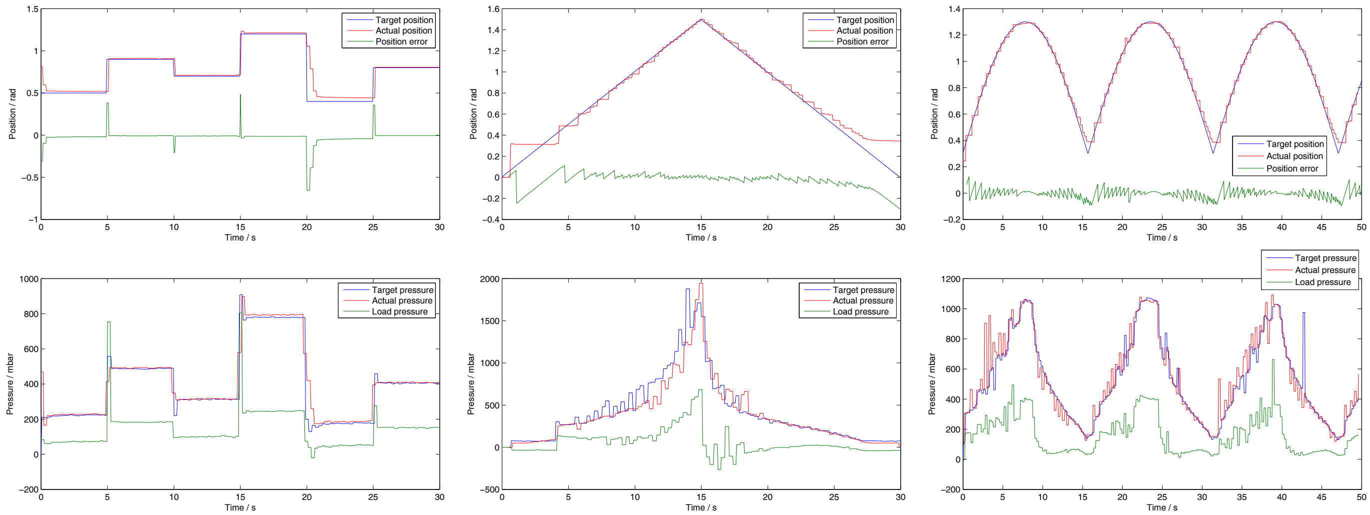

(a) Step response (b) Linear ramp function (c) Sine function

Fig. 7. Different system responses of the controlled actuator.

admitted to the actuator again.

During $(30s < t < 38s)$ the joint is disturbed in the positive angle direction, thus the position controller consequently reduces the pressure command for the underlying pressure control loop until the actuator is pressureless.

C. Experiments shown in attached video

In the attached video the FRH-4 hand is mounted to the humanoid robot Armar-III [12] which supplies the hand with a small air compressor located in its mobile base. The first part of the video shows two repetitions of a joint angle trajectory sequence comprising all finger joints in real-time. The finger joints are sequentially closed, moving to a final target angle of 1 rad and then opened again in reverse order. The joint angle values are interpolated linearily to produce a smooth motion. It can be seen that the pneumatically coupled joints of ring and pinkie do not move synchronously, which is by design as all four actuators of these fingers are due to space restrictions currently controlled by a single pair of valves and therefore the airflow can not be controlled individually. The joint angle feedback is calculated as average value from all four position sensors. This example shows that individual active control for every joint is required for the future.

It can be seen that index and middle finger are moved to parallel configurations by the controller. The controller is tuned with a slight overshoot characteristic to allow a balanced compromise between fast response and precise following.

In the second part of the video the contact detection from load pressure estimation and forward kinematics as described in Sec. III-D is demonstrated. The fingers close at a predefined grasping position with a low force value $p_{\text{c,max}} = 2000 \text{ mbar}$ using a three-finger precision grasp and the robot checks if a contact was detected during closing the fingers. If this is the case, the hand is moved to a delivery position and the object is released.

V. CONCLUSIONS

In this paper we presented a force-position control scheme for the pneumatic actuators of an anthropomorphic robot hand. Our approach is based on a simplified model for the zero-load actuator characteristics to linearize major non-linearities of the system. The remaining model error consists mainly of a hysteresis and is compensated by a cascaded controller with an joint angle position controller as inner loop and a pressure controller as outer loop. Using this model we can compute the load pressure from pressure and position readings and detect fingertip contact situations. We have implemented our method on a microcontroller system controlling a pneumatic robot hand with 8 DoFs. We gave detailled report on the system response for different joint angle trajectories and the performance of the force control.

Concluding, the developed and implemented method enables us now to perform precise and compliant robotic grasping with the FRH-4 hand which has not been shown yet for this type of compact fluidic actuator. From the detailed investigation of the actuator which was required for modelling it is now possible to optimize several components of the system to improve control results. An obvious aspect is to investigate alternative methods for the retraction system in order to overcome the non-linear and time-varying characteristics of the elastic rubber band. This will reduce the joint angle hysteresis significantly. Further, it is desirable to deploy switching valves with a faster response time. This will also increase precision and response time of the controlled system.

We are planning to test the control algorithm on an enhanced version of the robot hand offering more valves and thus more DoFs, especially providing individual control of ring finger and pinkie. On the application side we will now start testing grasping and haptic exploration methods with Armar-III.

Acknowledgement

We would like to thank the FRH-4 developer team around Stefan Schulz at the *Institute for Applied Computer Science*, *Research Center Karlsruhe (KIT)* for their continuous support during this work.
The work described in this paper was conducted within the EU Cognitive Systems project PACO-PLUS (FP6-027657) funded by the European Commission.

References

[1] J. Butterfass, M. Grebenstein, H. Liu, and G. Hirzinger, “DLR-Hand II: next generation of a dextrous robot hand,” in *Proceedings on IEEE International Conference on Robotics and Automation*, vol. 1, 2001, pp. 109–114.

[2] C. Lovchik and M. Diftler, “The robonaut hand: a dexterous robot hand for space,” in *Proc. IEEE International Conference on Robotics and Automation*, M. Diftler, Ed., vol. 2, 1999, pp. 907–912.

[3] S. Jacobsen, E. Iversen, D. Knutti, R. Johnson, and K. Biggers, “Design of the Utah/M.I.T. dextrous hand,” in *Robotics and Automation. Proceedings. 1986 IEEE International Conference on*, vol. 3, 1986, pp. 1520–1532.

[4] R. Walker, “Design of a dextrous hand for advanced clawar applications,” in *Climbing and Walking Robots and the Supporting Technologies for Mobile Machines: CLAWAR 2003*. Shadow Robot Company, 2003, pp. 691–698. [Online]. Available: http://www.shadowrobot.com/

[5] I. Gaiser, S. Schulz, A. Kargov, H. Klosek, A. Bierbaum, C. Pylatiuk, R. Oberle, T. Werner, T. Asfour, G. Bretthauer, and R. Dillmann, “A new anthropomorphic robotic hand,” in *IEEE-RAS International Conference on Humanoid Robots*, 2008.

[6] B. W. Surgenor and N. D. Vaughan, “Continuous sliding mode control of a pneumatic actuator,” *Journal of Dynamic Systems, Measurement, and Control*, vol. 119, no. 3, pp. 578–581, 1997. [Online]. Available: http://link.aip.org/link/?JDS/119/578/1

[7] J. Bobrow and B. McDonell, “Modeling, identification, and control of a pneumatically actuated, force controllable robot,” vol. 14, no. 5, pp. 732–742, Oct. 1998.

[8] G. Carducci, M. Foglia, A. Gentile, N. Giannoccaro, and A. Messina, “Pneumatic robotic arm controlled by on-off valves for automatic harvesting based on vision localisation,” in *Proc. IEEE International Conference on Industrial Technology IEEE ICIT ’04*, vol. 2, 8–10 Dec. 2004, pp. 1017–1022.

[9] A. Gentile, N. Giannoccaro, and G. Reina, “Experimental tests on position control of a pneumatic actuator using on/off solenoid valves,” in *Proc. IEEE International Conference on Industrial Technology IEEE ICIT ’02*, vol. 1, 11–14 Dec. 2002, pp. 555–559.

[10] B. Vanderborght, B. Verrelst, R. van Ham, J. Vermeulen, and D. Lefeber, “Dynamic control of a bipedal walking robot actuated with pneumatic artificial muscles,” in *Proc. IEEE International Conference on Robotics and Automation ICRA 2005*, Apr. 18–22, 2005, pp. 1–6.

[11] S. Beck, R. Mikut, A. Lehmann, and G. Bretthauer, “Model-based control and object contact detection for a fluidic actuated robotic hand,” in *Proc. 42nd IEEE Conference on Decision and Control*, R. Mikut, Ed., vol. 6, 2003, pp. 6369–6374.

[12] T. Asfour, K. Regenstein, P. Azad, J. Schroder, A. Bierbaum, N. Vahrenkamp, and R. Dillmann, “Armar-III: An integrated humanoid platform for sensory-motor control,” in *Humanoid Robots, 2006 6th IEEE-RAS International Conference on*, Dec. 2006, pp. 169–175.